A versatile bioink for three-dimensional printing of cellular scaffolds based on thermally and photo-triggered tandem gelation

A versatile bioink for 3D printing of cellular scaffolds based on thermally and photo-triggered tandem gelation

Matti Kesti[a†], Michael Müller[a†], Jana Becher[b], Matthias Schnabelrauch[b], Matteo D'Este[c], David Eglin[c], Marcy Zenobi-Wong[a]*

a) Cartilage Engineering + Regeneration Laboratory, ETH Zürich, Otto-Stern-Weg 7, 8093 Zürich, Switzerland
b) Biomaterials Department, INNOVENT e.V. Jena, Prüssingstrasse 27 B, 07745 Jena, Germany
c) AO Research Institute Davos, Clavadelerstrasse 8, 7270 Davos Platz, Switzerland

*Corresponding author. Marcy Zenobi-Wong, Cartilage Engineering + Regeneration, Department of Health Science & Technology, ETH Zürich, Otto-Stern-Weg 7, HPL J22, 8093 Zürich, Switzerland. Phone: +41 44 632 50 89, Fax: +41 44 633 11 94, email: marcy.zenobi@hest.ethz.ch;

† Both authors contributed equally to this publication

Keywords: Bioprinting, HA-pNIPAAM, Thermoresponsive Polymer, Cartilage Engineering

Abstract

Layer-by-layer bioprinting is a logical choice for the fabrication of stratified tissues like articular cartilage. Printing of viable organ replacements, however, is dependent on bioinks with appropriate rheological and cytocompatible properties. In cartilage engineering, photocrosslinkable glycosaminoglycan-based hydrogels are chondrogenic, but alone have generally poor printing properties. By blending the thermoresponsive polymer poly(*N*-isopropylacrylamide) grafted hyaluronan (HA-pNIPAAM) with methacrylated hyaluronan (HAMA), high-resolution scaffolds with good viability were printed. HA-pNIPAAM provided

fast gelation and immediate post-printing structural fidelity, while HAMA ensured long-term mechanical stability upon photocrosslinking. The bioink was evaluated for rheological properties, swelling behavior, printability, and biocompatibility of encapsulated bovine chondrocytes. Elution of HA-pNIPAAM from the scaffold was necessary to obtain good viability. HA-pNIPAAM can therefore be used to support extrusion of a range of biopolymers which undergo tandem gelation, thereby facilitating the printing of cell-ladened, stratified cartilage constructs with zonally-varying composition and stiffness.

1. Introduction

Healthy articular cartilage allows almost frictionless movement of the synovial joints. Focal lesions in the tissue resulting from high impact mechanical loading from sports injuries or trauma will not be repaired spontaneously due to the limited healing capabilities of cartilage and may progress to include degeneration of the surrounding tissue [1, 2]. Hence, surgical interventions are necessary to repair damage of the articular cartilage surface. One clinical treatment for large cartilage defects is osteochondral transplantation or mosaicplasty, where the cartilage lesion is filled with an array of tightly-packed cylinders of osteochondral grafts. Although this technique may allow increased weight bearing [3, 4], it is hampered by several disadvantages including scarcity of tissue, donor site morbidity (for autologous grafts), potential transfer of disease (for allogenic grafts), and poor integration with the host tissue and between cylinders. Another main disadvantage is the unavoidable mismatch in thickness and curvature between the donor cylinders and implantation site. The fabrication of individual cell-ladened osteochondral grafts whose geometry is obtained from MRI data would have enormous advantages over the current clinical option.

Bioprinting is a natural fabrication method given the stratified nature of articular cartilage, and could improve the functionality tissue engineered scaffolds by allowing the placement of cells [5-7], biomaterials [8-10] and bioactive cues [11-13] in three dimensional space to mimic the native tissue.

However the search for bioinks for use in tissue printing applications [14, 15] which has both good biocompatibility and tailored viscosity transitions for effective printing and handling continues [16, 17]. For an extrusion based process, the bioink should show shear thinning to allow extrusion through a needle and also immediate cessation of flow upon deposition on the substrate to retain its plotted shape. Such a material would allow the fabrication of complex structures with high resolution [18, 19]. The final mechanical properties of the printed construct should also be sufficient for manipulation. The different stages of a biofabrication process and the viscosity requirements for an ideal bioink are shown in Fig. 1b. Bioinks such as alginate-gelatin blends [20, 21] or pure alginate [20] have been used to generate 3D scaffold structures. These materials have the advantage of good biocompatibility and cell friendly ionic/thermal crosslinking without further chemical modifications of the biopolymers. However, these materials are usually soft and their mechanical properites decrease over time due to the reversibility of the non-covalent crosslink. It has been reported that the initial modulus of alginate-gelatin (10 kPa) scaffolds decreased over 60% in 7 days in culture [20]. Due to the limitation of these materials, interest in covalently crosslinked hydrogels has been increasing. Bioinks comprising of polymers modified with (meth-)acrylates or diacetate have been extensively studied for biofabrication purposes. These modifications have been conjugated to both natural and synthetic polymers to create methacrylated gelatin (GelMA) [18, 22] and acrylated versions of polymers such as poloxamer [23] and poly (ethylene glycol) [24]. The biggest advantage of the GelMA based bioinks is the good biocompatibility and improved mechanical properties with a compression modulus around 180 kPa after 30min of UV exposure [22]. For a more extensive review on the subject, the reader is referred to the recent review from Malda *et al.* [25].

As natural components of articular cartilage, hyaluronan and chondroitin sulfate are logical material choices for cartilage tissue engineering [26-29]. Both are used clinically as injections or food supplements and have purported anti-inflammatory [30-32] and/or immunomodulatory effects [33]. Bioprinting of glycosaminoglycan-based hydrogels, however, is challenging as the precursor solutions

of these materials often have low viscosity and slow gelation kinetics which result in flow before gelation. The goal of this study was to investigate the possibility of utilising natural cartilage components hyaluronan and chondroitin sulfate in bioprinting. We hypothesized that a fast, reversible gelling component could be added to methacrylated hyaluronan and chondroitin sulfate to enhance their printing. Poly(*N*-isopropylacrylamide) (pNIPAAM) conjugated to hyaluronan (HA) was chosen as a thermoresponsive polymer as good cytocompatibility has been reported with nucleus pulposus cells [34], mesenchymal stromal cells [35] and a fibroblast cell line [36]. By grafting pNIPAAM onto the HA backbone (Fig. 1c), thermoresponsive hydrogels were created that are liquid at room temperature and gel at body temperature [37, 38]. The basis of this gelation is the lower critical solution temperature (LCST) of pNIPAAM which is around 32°C [39]. The liquid state allows easy loading of the cartridges of the bioprinter and simplifies the mixing of cells, additional polymers and growth factors, whereas rapid gelation upon deposition onto a heated substrate ensured the maintenance of the shape of the printed 3D structure until the further crosslinking (Fig. 2). After stabilization of the biopolymer with free radical polymerization of the HAMA, the HA-pNIPAAM can be eluted leaving a glycosaminoglycan-based scaffold (Fig. 2).

2. Materials and Methods

2.1 Materials

2,2-azobisisobutyronitrile (AIBN), *N*-isopropylacrylamide (NIPAAM) monomer, *N,N*-dimethylformamide (DMF), 2-aminoethanethiol hydrochloride, diethyl ether, Dowex Resin M-31, tetrabutylammonium hydroxide (TBA-OH), dimethyl sulfoxide (DMSO), carbonyl diimidazole (CDI), sodium bromide (NaBr), pronase, collagenase, methacrylic anhydride, L-ascorbic acid, sodium hydroxide (NaOH) were all purchased from Sigma Aldrich (Buchs, Switzerland). Chondroitin sulfate (CS, DS_S (degree of substitution (sulfate groups)) = 0.9, M_W = 20 kDa, polydispersion index M_w/M_n = 1.55) was purchased from Kraeber (Ellerbek, Germany). Lithium phenyl-2,4,6-trimethylbenzoylphosphinate (LAP) was prepared following the procedure reported by Fairbanks *et al.* [40]. Dulbecco's modified Eagle's media (DMEM), phosphate buffered saline (PBS), fetal bovine

serum (FBS), antibiotic-antimycotic, Live/Dead Assay, and trypsin/EDTA were all purchased from Life Technologies (Zug, Switzerland). High molecular weight hyaluronan sodium salt (HANa, 1506 kDa, M_w/M_n = 1.53) and low molecular weight HANa (293 kDa, M_w/M_n = 1.86) was obtained from Contipro Biotech s.r.o (Dolni Dobrouc, Czech Republic). All dialysis membranes used were from SpectrumLabs (Breda, Netherlands) and the 3-(trimethylsilyl)-1-propanesulfonic acid sodium salt (MTS) assay was from Promega (Madison, USA). Methanesulfonic acid was obtained from Fluka (Buchs, Switzerland). Alginate (ProNova UP-LVG) was purchased from NovaMatrix (Sandvika, Norway).

All concentrations are given in percentages weight/volume (% w/v) unless indicated otherwise.

2.2 Synthesis of polymers

2.2.1 pNIPAAM-NH2 synthesis

Amino-terminated pNIPAAM (pNIPAAM-NH2) was synthesized by radical polymerization using AIBN as a radical initiator [41]. Briefly, NIPAAM monomer (1.13 g) was dissolved in degassed DMF together with AIBN (1.6 mg) and 2-aminoethanethiol hydrochloride (11.4 mg). The polymerization was carried out at 70°C for 6 h under argon atmosphere. The reactant was precipitated in an excess of diethyl ether and dried under vacuum at room temperature. The precipitate was dissolved in ultrapure water and dialyzed for 48 h (Spectra/Por 7, MWCO 8000 Da) in ultrapure water. The dialyzed product was then lyophilized, characterized and stored until further use.

The molecular weight of the synthesized pNIPAAM was determined using a multi-detector chromatographic system (GPCV 2000, Waters, Milford, USA) equipped with three online detectors: a differential viscometer, a differential refractometer and a multi-angle light scattering (MALS) Dawn DSP-F photometer (Wyatt, Santa Barbara, USA). The mobile phase was DMF + 0.1 M LiCl with a flow rate of 0.8 mL/min, 50°C and an injection volume of 218.5 µL. The sample concentration was 2 mg/mL. Evaluation of the molecular weight of the synthesized polymer was 24 kDa for the pNIPAAM.

2.2.2 HA-pNIPAAM synthesis

15 g of HANa was dissolved in 1.1 L of ultrapure water under constant stirring. Dowex Resin M-31 (120 g) was washed with ultrapure water until the washing solutions were clear and further soaked overnight in ultrapure water. Water was then removed from the resin and covered with 70 g of a 40% TBA-OH water solution. The solution with the resin was placed on an orbital shaker for 1 h, after which the supernatant was removed and replaced with 80 g of fresh TBA-OH solution and placed overnight on an orbital shaker. After that, the resin was rinsed with large amounts of ultrapure water until the flow through was clear and the pH was below 10. The resin was then moved into a gooch filter (N°2) and water was removed without drying out the resin. The filter containing the resin was then filled with the HANa solution. The solution was left to flow through the resin and finally collected and frozen at -20°C. The product was freeze dried and subsequently further dried at 42°C under vacuum.

2 g of HA-TBA was then dissolved in 160 ml of DMSO. pNIPAAM-NH2 (3.5 g) was dissolved in 40 mL of DMSO. First, 230 µL of methanesulfonic acid and then 540 mg of CDI were added to the dissolved HA-TBA and stirred at 42°C for 1 h. After that, the pNIPAAM-NH2 solution was added and the mixture was cooled down to room temperature and the reaction was let to proceed for 48 h under constant stirring. Then 20 mL of saturated NaBr solution was added dropwise until the reaction mixture turned cloudy and stirred for another 2 h at room temperature. The solution was then transferred into dialysis tubing (Spectra/Por 6 RC, MWCO 50 kDa) and dialyzed against cold (< 13°C) tap water which was changed every 30 min within the first 4 h. The dialysis was continued against ultrapure water for 24 h with changing the water twice daily and then for another 3 days with daily changes of water. The polymer was freeze-dried and further dried at 42°C under vacuum for 3 days.

The molecular weight of HA was evaluated by utilizing the same setup as for the pNIPAAM-NH2 (Section2.2.1). The mobile phase was 0.2 M NaCl with a flow rate of 0.4 mL/min, 35°C and an injection volume of 150 µL. The sample concentration was 0.1 mg/mL. The molecular weight found was 1506 kDa for the HA. Using this value and the molecular weight of pNIPAAM, the grafting density

of pNIPAAM on HA was estimated by integrating the peak of the methyl groups of pNIPAAM at 1.14 ppm and dividing the integrated value of the peaks of HA at 3.00 - 3.77 ppm. The calculated grafting density was 4.6 % which is comparable to values in the literature [38].

2.2.3 HA methacrylation

1% low molecular weight HA was dissolved into ultrapure water with gentle agitation. The pH was adjusted to 8 with NaOH. A 20 fold molar excess (per disaccharide unit) of methacrylic anhydride was added under vigorous stirring and the reaction was allowed to proceed in an ice bath for 24 h. The pH was kept constant during the first three hours of the reaction by adding 5M NaOH drop wise. After 24 h the reactant was precipitated into an excess of ethanol and the precipitate was collected by vacuum filtration. The dried precipitate was dissolved in ultrapure water and dialyzed for three days against ultrapure water (Spectra/Por 5, MWCO 12-14 kDa). The water was changed every 24 h. The product was freeze-dried and further dried at 42°C under vacuum for 24 h and stored at -20^{o}C before use. NMR spectroscopy revealed successful methacrylation of the hyaluronan. The degree of substitution (DS_{MA}) was calculated by the ratio of the integrals of the vinyl protons at 5.6 ppm and 6.1 ppm to the protons from the methyl groups of both, HA and the methacryl residues at 1.9 ppm. The calculated degree of substitution was 0.3 (out of 4 hydroxyl group per disaccharide repeat unit).

2.2.4 CS methacrylation

2% CS was dissolved in borate buffer (pH = 8.5) and reacted with a 15-fold excess methacrylic anhydride per disaccharide repeating unit at 5°C. The pH was constantly adjusted to 8 with NaOH. After a reaction time of 24 h the solution was precipitated into an excess of acetone and the precipitate was collected by vacuum filtration. The dried precipitate was dissolved in water and dialyzed (MWCO 3 kDa) against water. The water was changed 2 – 3 times per day. The product was isolated by lyophilization and further dried at 40°C under vacuum for 8 h. The degree of substitution ($DS_{MA)}$ was determined from the ratio of the proton signals at 5.7 ppm and 6.1 ppm (vinyl protons),

and 1.9 ppm (methyl groups) in ^{1}H-NMR to be 0.5 (out of 3 hydroxyl group per disaccharide repeat unit).

2.3 Material characterization

2.3.1 Rheology

An Anton Paar MCR 301 (Anton Paar, Zofingen, Switzerland) rheometer equipped with a Peltier element for temperature control, a thermostatic hood and a UV Source (Omnicure Series 1000, 365 nm wavelength, 9.55 mW/cm^2) (Lumen Dynamics, Mississauga, Canada) was used. All measurements were performed with a cone-plate geometry (diameter 50 mm, angle 1°) under water vapor saturated atmosphere. The shear recovery experiments were performed by measuring G' and G'' at a frequency of 1 rad/s and 1% strain (which was established to be within the linear viscoelastic range), then shearing the sample for 1 second at 100 s^{-1} before returning to the oscillatory measurement. For the temperature gelation experiments, oscillatory measurements were performed at a frequency of 1 rad/s and 1% strain. The samples were first equilibrated at 4°C for 5 min and then heated at a rate of 0.5°C/min from 4°C to 40°C in case of the pure HA-pNIPAAM samples and from 4°C to 45°C in case of the two bioinks HAMA-HA-pNIPAAM and CSMA-HA-pNIPAAM. The gelation temperature was taken as the temperature where the storage modulus G' and the loss modulus G'' are equal. UV crosslinking was performed subsequently for 5 min at 37°C (after 5 min equilibration time) with 50% maximum intensity and 3.5 cm distance between the source and the sample.

2.3.2 Swelling

For the equilibrium swelling experiments, gels of 50 µL (n=5) were created for the two different bioinks. The gels were immersed in 1 mL of PBS at either 4°C or 37°C and incubated for 0.5, 1, 4, 24 and 48 h. After all incubation periods, PBS was removed and the gels were weighed ($m_{Swollen}$). The gels were then subsequently lyophilized and weighed again (m_{Dry}). The swelling ratio Q was then calculated as

$$Q = \frac{m_{Swollen} - m_{Dry}}{m_{Dry}}$$

2.4 Cell culture

Bovine chondrocytes were harvested from full thickness articular cartilage from the lateral and medial femoral condyle of 6 month old calves obtained from the local butcher. The cartilage slices were minced with a surgical blade and the tissue slices were digested for 4h with 0.2% pronase in DMEM supplemented with 1% antibiotic-antimycotic in an incubator (37°C, 5% CO_2) under gentle stirring. Following this first digestion step, the tissue was further digested for 6h with 0.03% collagenase in DMEM supplemented with 1% antibiotic-antimycotic under gentle stirring. The tissue was then filtered first through a 100 µm cell strainer and subsequently through a 40 µm cell strainer. Cell viability was found to be above 90%. Passage 0 cells were seeded at 10'000 cells/cm^2 in DMEM containing 10% fetal bovine serum, 1% antibiotic-antimycotic and 50 µg/mL L-ascorbic acid. This media formulation was used in all further experiments. Cells were passaged until passage 4 before encapsulation. Each passage was done at 80% confluency utilizing trypsin/EDTA and reseeded at 5000 cells/cm^2. The media was changed every 3 days.

2.4.1 Top culture of hydrogels

HA-pNIPAAM was dissolved in PBS and mixed together with chondroitin sulfate (CSMA) methacrylate or hyaluronan methacrylate (HAMA). The mixing was done at 4°C to avoid gelation of the HA-pNIPAAM. As a photoinitiator for the UV crosslinking, lithium phenyl-2,4,6-trimethylbenzoylphosphinate (LAP) was added at a concentration of 0.05%. Hydrogel solutions of 200 µL volume were placed at the bottom of a 24-well plates and crosslinked for 15 min in an incubator (37°C, 5% CO_2) prior to further crosslinking by utilizing a hand held UV source (365 nm wavelength, 22 mW/cm^2, Blak-Ray B-100AP, UVP, United States) for 5 min. Passage 4 bovine chondrocytes were seeded on top of the hydrogels at 2 x 10^4 cells/well. Chondrocytes were left to adhere for 2 h in the incubator before additional media was added. 1% alginate gels were prepared

with the $CaCl_2$ gelation method as a positive control according to established methods [42, 43]. Media was changed every 3 days.

2.4.2 Cell encapsulation and printing

Bioprinting of the scaffolds was performed using a BioFactory (regenHU, Villaz-St-Pierre, Switzerland) equipped with a needle with an inner diameter of 300 µm. Temperature of the cartridges was controlled with a syringe heating pad and a temperature control unit (New Era Pump Systems, Farmingdale, USA). All printing was performed onto a heated substrate with a surface temperature between 35°C and 38°C. The printer was also equipped with a UV-PEN (wavelength 365 nm, 6.09 mW/cm^2) that was used to crosslink each printed layer for 10 s. The spacing between the center of the printed strands was 2 mm. Printing parameters were optimized by changing the pressure and writing speed to minimize strand diameter. The scaffolds were drawn with the BioCAD software (regenHU, Villaz-St-Pierre, Switzerland) and converted into ISO code for the printing process.

Materials were prepared as described in Section 2.4.1 at a concentration of 15% HA-pNIPAAM and 2% HAMA. The bioink was stirred gently and mixed with the 0.05% LAP solution prior to cell encapsulation. Passage 4 bovine chondrocytes were mixed with the bioink at a concentration of $6x10^6$ cells/ml at 4°C to avoid gelation of HA-pNIPAAM. The cell-containing bioink was then transferred into the printing cartridge and scaffolds printed (n=3). Printing was performed in the BioFactorys in-built biosafety cabinet and all parts involved in the printing process were sterilized with 70% ethanol prior to the cell printing. A pressure of 1.5 Bar and a feed rate of 500 mm/min were used for the printing of the scaffolds. The thickness of a single layer was 200 µm when no cells were added and 210 µm with the addition of cells. When cells were encapsulated in the bioinks, five consecutive layers were printed resulting in 1.05 mm thick scaffolds. The total volume of each construct was calculated to be 77 µL containing 4.6×10^5 cells. The scaffolds were transferred into culture media either at 37°C or, to elute the HA-pNIPAAM, at 4°C. The scaffolds at 4°C were kept at this temperature for 30 min while changing the media every 10 min. After washing, the scaffolds were incubated in the same conditions as the other scaffolds (37°C, 5% CO_2). 1% alginate gels of the

same volume and cell concentration as the printed constructs were prepared with the $CaCl_2$ gelation method and used as the positive control. Media was changed after 3 days. Cell viability was assessed after 4 days culture.

2.4.3 Cell viability analysis

Cell viability was assessed using a Live/Dead with viable cells stained green and dead cells stained red fluorescent. Staining was performed with a 2 µM Calcein AM-4 µM ethidium homodimer solution for 25 min for the top culture and 1 h for the encapsulated cells. The cells were imaged with a fluorescent microscope (Zeiss Axio Observer, Zeiss, Switzerland) and images were evaluated with Image J software. Each condition was done in triplicate and 3 images were taken from each sample. In addition, cell viability was further investigated using the 3-(4,5-dimethylthiazol-2-yl)-5-(3-carboxymethoxyphenyl)-2-(4-sulfophenyl)-2H-tetrazolium inner salt (MTS) assay according to the manufacturer's protocol.

2.5 Statistical analysis

Data from the MTS viability assays is expressed as mean ± standard deviation. Statistical analysis of the MTS data was performed using a one-way ANOVA and Bonferroni post-hoc testing (OriginPro 8.5, OriginLab) and significance was determined at $p < 0.05$.

3. Results

3.1 Bioink characterization

3.1.1 Rheological characterization

To determine the HA-pNIPAAM concentration most suitable for blending with the two methacrylated biopolymers CSMA and HAMA, HA-pNIPAAM solutions of 10%, 15% and 20% were examined with rheometry. The viscoelastic moduli of different concentrations of pure HA-pNIPAAM (Fig. 3a) as a function of temperature show that the gelation temperatures for all concentrations were between 25.7°C and 29.7°C. This is lower than the LCST of pure pNIPAAM (32°C), however, the maximal

increase in G' for all three concentrations still takes place around the LCST of pure pNIPAAM. The 10% HA-pNIPAAM shows the lowest final storage modulus from all three tested concentrations with G' being 134 Pa. The storage modulus of the two higher concentrated HA-pNIPAAM solutions are both one order of magnitude higher than 10% HA-pNIPAAM, namely 3000 Pa for the 15% HA-pNIPAAM and 4450 Pa for the 20% HA-pNIPAAM solution. Although the storage moduli of the two higher concentrated HA-pNIPAAM solutions are of the same order of magnitude, we chose the 15% HA-pNIPAAM solution as the concentration in our bioinks as its gelation temperature is higher (20% solution G' = G'' at 25.7°C and 15% solution G' = G'' at 29.7°C). With the gelation temperature further away from room temperature, the risk of undesired gelation is minimized. Furthermore, its lower viscosity below the gelation temperature allows easier handling than with the 20% HA-pNIPAAM solution.

To further investigate if the 15% HA-pNIPAAM solution would be suitable as a base material for a bioink, the solution was tested at three different temperatures for its ability to quickly recover after shear. The shear recovery simulates the shear forces the bioink experiences when extruded through the needle during the printing process. Immediate recovery after exiting the needle is necessary to avoid flow of the bioink and ensure accurate printing. Fig. 3b shows the recovery of 15% HA-pNIPAAM after shear, with the storage modulus normalized to the initial storage modulus (before shear) at three different temperatures. At 4°C, below the gelation temperature, the HA-pNIPAAM solution is a liquid and the G' value recovers quickly after shear to its initial value (5 Pa). When performing the shear recovery experiment at elevated temperatures below and above the LCST, namely 23°C and 37°C, the storage modulus does not recover as completely as in the case of the HA-pNIPAAM at 4°C. For HA-pNIPAAM at 37°C, the storage modulus G' only recovers to 8.5% of its initial value of 2131 Pa. When the temperature is lowered to 23°C (approximately 6°C below the gelation temperature), the liquid recovers quickly to 88% of its initial value of 8 Pa. After this initial rise in G', the modulus keeps increasing over time, reaching 120% of its initial value after 1000 seconds. We

therefore decided to use 23°C as the printing temperature for the bioprinter components, except for the heated stage (35°C - 38°C).

Tandem gelation behavior was analyzed with and without the addition of cells to the different HA-pNIPAAM biopolymer blends. The term tandem gelation refers to the initial physical temperature gelation followed by chemical crosslinking utilizing a UV source. 5% chondroitin sulfate methacrylate (CSMA-HA-pNIPAAM bioink) was added whereas hyaluronan methacrylate (HAMA-HA-pNIPAAM bioink) was added at 2% as larger amounts did not dissolve well or increased the viscosity of the solution to an extent where pipetting was no longer possible. The bioinks were tested for their gelation temperature and UV crosslinking behavior. In both cases, the addition of the biopolymers led to an increase in both G' and G'' compared to pure 15% HA-pNIPAAM at temperatures below the LCST. At low temperatures, the biopolymers caused the G' value of both blends to be larger than the G'' value, which is normally attributed to gel-like materials. However, we observed that the bioinks were still liquid at 4°C. We believe that the additional polymer content shifted the frequency spectra of the bioink to lower frequencies compared to pure HA-pNIPAAM i.e. the crossover of G' and G'' in the frequency spectra is found at frequencies < 1 rad/s. It is therefore no longer possible to define a clear gelation temperature according to G' = G'', but an increase in G' indicates that crosslinking of the pNIPAAM chains still takes place. We thus compared the maximum increase of G' of the bioinks, rather than the gelation temperature. In the CSMA-HA-pNIPAAM bioink, the addition of the biopolymer lowers the storage as well as the loss modulus achieved after the temperature gelation whereas the maximum increase of the modulus appears at a slightly earlier time point (58.48 min or at 30.5°C) than for the pure HA-pNIPAAM sample (61.48 min or at 32.0°C Fig. 3c). In case of the HAMA-HA-pNIPAAM bioink, the maximum increase of the modulus appears at slightly later time (62.05 min or at 32.3°C). The values for G' and G'' are reduced in comparison to the pure HA-pNIPAAM with a G' value of 6.32 Pa for the CSMA bioink after temperature crosslinking instead of 3220 Pa. At 10% CSMA addition, the ability of HA-pNIPAAM to form a gel is completely lost (data not

shown). A similar effect is observed for the HAMA-HA-pNIPAAM bioink, however, the decrease in the G' value (1210 Pa) is not as large as in the case of CSMA-HA-pNIPAAM bioink.

As the final bioinks will contain cells, we also investigated the influence of cells on the gelation behavior of our bioinks. When cells (6×10^6/ml) are embedded into the bioinks, the G' and G'' values of the CSMA-HA-pNIPAAM bioink at temperatures below the LCST decreased whereas for the HAMA-HA-pNIPAAM bioink the G' and G'' values increased. The sharp increase in G' appears at a later time point for CSMA-HA-pNIPAAM when cells are added, namely 1.6 min later (60 min, 31.3°C) than the blend without any cells, which corresponds to a temperature difference of 0.8°C. In the case of the HAMA-HA-pNIPAAM bioink, the maximum increase in G' and G'' takes place at an earlier time point with added cells (60 min or at 31.3°C). The final values of G' and G'' after temperature gelation are lowered upon the addition of cells. The UV crosslinking procedure was not inhibited by the cells and the final storage moduli after crosslinking exhibited no large changes in case of the CSMA-HA-pNIPAAM with a G' of 3165 Pa compared to 2750 Pa when the cells were added. The storage modulus of the HAMA-HA-pNIPAAM blend after UV crosslinking (2532 Pa) was increased when the cells were added (8370 Pa).

3.1.2 Swelling

Swelling of both bioinks was investigated in PBS at 4°C and 37°C i.e. below and above the LCST of pNIPAAM. Swelling at 4°C led in both bioinks to an initial increase of the gel weight within the first 4 h of the swelling experiment as shown in Fig. 4. The HAMA-HA-pNIPAAM bioink increased from a swelling ratio of 11.4 up to a maximum of 22.7 after 24 h, after which time the swelling stayed constant (Fig. 4a). The same behavior is seen in the CSMA-HA-pNIPAAM bioink where the swelling ratio changed from 17.8 after 0.5 h to a maximum of 29.1 after 24 h (Fig. 4b). As with the HAMA-HA-pNIPAAM bioink, the swelling ratio did not change after this. When the samples are swollen at 37°C, neither of the bioinks shows a weight gain within the first 4 h like observed at 4°C. As HA-pNIPAAM is leaving the gels at 4°C, water can enter and the swelling ratio increases. This effect is not seen at

37°C as HA-pNIPAAM is in its gelled state and not able to be eluted. At both temperatures, the CSMA-HA-pNIPAAM bioinks show a larger swelling ratio than the HAMA-HA-pNIPAAM bioinks.

3.2 3D printing of constructs

Scaffolds were printed with the HAMA-HA-pNIPAAM bioink as it showed a higher storage modulus after temperature gelation compared to CSMA-HA-pNIPAAM. We expected therefore the best printing properties from this bioink as it was the most likely to show complete cessation of flow upon deposition onto the heated substrate. The high storage modulus was important for the material to withstand the printing of additional layers. To evaluate the influence of the writing speed and the printing pressure on the strand diameter, single lines were printed onto a heated substrate with different combinations of writing speed and pressure and subsequently evaluated with a microscope. The strand diameter is preferably as thin as possible as thick strands limit the diffusion of nutrients and oxygen to the cells embedded within. The thinnest strand which could be continuously extruded had a width of 620 µm and was achieved with a writing speed of 500 mm/min at a printing pressure of 1.5 bar. These parameters were then further utilized for the printing of the scaffolds. The layer thickness was determined empirically by printing lines on top of each other and visually observing the position of the needle at the start of every new line: a needle found to be above the lines indicated that the layer thickness was chosen too big whereas if the needle was printing within the previously printed line, the layer thickness was increased. For the printing parameters indicated above, we found that the strands produced had a layer thickness of 200 µm (210 µm with the addition of cells). We were able to produce scaffolds such as the ones shown in Fig. 5, with a diameter of 10 mm and a height of 2.8 mm, which represents the printing of 14 subsequent layers. Thinner scaffolds of 1.05 mm were printed for the cell-containing scaffolds to minimize production time and avoid drying effects. The initial thermal gelation in combination with the UV-crosslinking produced mechanically stable scaffolds that could be easily handled with a spatula (Fig. 5c) without breaking.

3.3 Cell viability

3.3.1 Cell viability in top culture

Bovine chondrocytes were cultured for seven days on top of the bioink hydrogels prior to Live/Dead and the MTS assays. Fig. 6a shows a viability of 98% in the Live/Dead assay for the 15% HA-pNIPAAM samples and therefore confirms earlier findings by other groups employing this hydrogel [34, 35]. Chondrocytes were not distributed evenly over the substrate but instead formed clusters on top of the HA-pNIPAAM. Cluster formation was also observed when the cells were cultured on top of the HAMA-HA-pNIPAAM bioink (Fig. 6b) but to a lesser extent. The cell viability on top of this bioink was lower than on top of pure HA-pNIPAAM. In the case of the CSMA-HA-pNIPAAM bioink only a few of the cells initially seeded were still attached after seven days (Fig. 6c). The observations from the Live/Dead assay were confirmed by the MTS assay where a 1% alginate gel was used as a positive control. The assay shows a low absorbance for the CSMA-HA-pNIPAAM bioink which reflects the low cell attachment. For the 15% HA-pNIPAAM, the absorbance was at a similar level to the alginate control. The HAMA-HA-pNIPAAM bioink showed a lower absorbance which is in agreement with the lower viability seen in the Live/Dead assay.

3.3.2 Viability of cells encapsulated within bioink hydrogels

To test the viability of the chondrocytes in the hydrogels after printing, cells were encapsulated in the HAMA-HA-pNIPAAM bioink and scaffolds were printed. The control group of chondrocytes encapsulated in alginate had excellent viability (Supplementary Figure S1) and showed no toxicity upon exposure to equivalent amounts of ultraviolet light used in the printing process (Supplementary Figure S2). After 4 days, the MTS assay (Fig. 7a) of the printed constructs (before removal of HA-pNIPAAM at 4°C) revealed a very low viability. However, after washing the printed constructs, the viability of the chondrocytes improved dramatically (Fig. 7a). The cells were mostly viable throughout

the printed structure (Fig. 7b and c), however, there was increased cell death around the pores of the construct (Fig 7b).

When washed with cold PBS, the constructs lost their opaque appearance (Fig. 7d), indicating the HA-pNIPAAM was no longer in its gelled state and could therefore diffuse out of the scaffold. The final scaffold therefore consisted mainly of the UV-crosslinked biopolymer. In this regard, the HA-pNIPAAM serves as a temporary support matrix that can be sacrificed after UV-crosslinking of the second component of the bioink.

4. Discussion

Bioprinting is a technique which can be used to create biomimetic layered constructs for cartilage engineering through its ability to spatially distribute hydrogels, cells and bioactive molecules at pre-defined sites. However, the need for different viscosities at different stages of the printing process has limited the choice of materials suitable for bioprinting. In 3D printing the required viscosity changes can be achieved by a transition from melts to solids or by evaporation of an organic solvent, however, these approaches cannot be used in the presence of cells and biological materials. Fast thermal gelation of certain biocompatible polymers on the other hand can be achieved by deposition of small volumes onto heated or cooled substrates [18, 44]. Gelatin is such a material, but requires temperatures above 37°C to maintain the liquid state. Gelatin methacrylate has excellent printing properties [16, 18, 22], however, it is not reversible at physiological temperatures and contains denatured animal protein. The inverse thermoresponsive polymer HA-pNIPAAM has the advantage of an LCST around body temperature and its gelation is reversible by simple cooling. HA-pNIPAAM is easy to handle at room temperature while gelling instantaneously when deposited onto a heated (37°C) substrate. Here we employed HA-pNIPAAM as a transient matrix to ensure cessation of flow upon co-deposition with photocrosslinkable biopolymers. Although tandem gelation has been used for injectable or printable hydrogels [44, 45], this is one of the first applications of tandem gelation in bioprinting based on a reverse thermoresponsive polymer.

It is important to consider the rheological behavior of inks for bioprinting due to the fact that they are exposed to a shear field when being extruded from the cartridge to the substrate. After the exposure to the shear forces in the needle during printing, the bioink should recover quickly. It is therefore necessary that any structure that is present in the ink at printing temperature quickly be rebuilt when the ink arrives on the substrate. This is normally valid for non-crosslinked polymer solutions [46]. In the case of HA-pNIPAAM, this seems to be the case for the printing temperatures (temperature of the cartridge and the needle) of 4°C and 23°C, but not for the printing at 37°C (Fig. 3b). At the latter temperature, structures that are present prior to extrusion are not present after the printing process, which is seen in the low recovery of the moduli after exposure to shear. The network formed by the interaction between the pNIPAAM chains at 37°C is fully developed and broken under shear. At 37°C, the pNIPAAM chains are hydrophobic and therefore collapse on themselves in the aqueous environment. As a consequence of this, individual pNIPAAM chains can no longer interact with each other and the reestablishment of the network is no longer possible. We suspect that the remaining 8% (Fig. 3b) of the initial storage modulus originate from chain entanglements and pNIPAAM chains that were not separated from each other upon shear. When the solution, on the other hand, is sheared at 4°C, the hydrated HA-pNIPAAM polymers do not interact when aligning themselves in the shear field. After shear, the molecules relax back to a coiled structure and the moduli return to the original values. The situation is again different at 23°C, where some of the pNIPAAM chains interact as indicated by the start of the increase of G' (Fig. 3a). We assume that this leads to the formation of small domains where several HA-pNIPAAM molecules interact with each other. These domains take longer to relax into the same state present before the exposure to shear, but are still able to align along the shear field without disrupting the pNIPAAM interactions. The continuous increase in the storage modulus up to 120% of the initial value could be either caused by shear induced structures that form slowly over time when the solution is at rest or the continuous formation of pNIPAAM crosslinks. As a saturated atmosphere was present in measuring chamber at all times, we can exclude drying effects. Although there was incomplete initial

recovery after shear at 23°C, this temperature was chosen as the printing temperature. If printed at 4°C, the sample would flow for too long before the temperature gelation was reached, thus reducing the resolution of the printing process. Even when printed at 23°C, some flow before complete gelation of the strands was still present as revealed by the difference in strand width (620 µm) and strand height (200 µm).

Ideal bioinks for 3D bioprinting should not only maintain their shape when at rest (i.e. possess a yield point), but should also be mechanically stable. In the case of HA-pNIPAAM, the gels are strong enough to maintain their shape after thermal gelation but do not withstand mechanical compression. The addition of a second polymer that can be covalently crosslinked to form a network within the HA-pNIPAAM gel is an elegant solution to create a mechanically stable gel. The addition of the two biopolymers used in this study, HAMA and CSMA, influenced the gelation temperature as our results demonstrate (Fig. 3c). Both biopolymers lower the storage modulus of the bioink after the thermal gelation process which is most probable due to steric hindrance between the pNIPAAM chains caused by the biopolymers. In addition, specific chemical interactions between the biopolymers and the pNIPAAM side chains might also play a role. The partial inhibit of pNIPAAM crosslink formation by the biopolymer addition effectively sets a limit to the amount of biopolymer the bioink can contain. The drop in the storage modulus of HA-pNIPAAM after temperature gelation might be proportional to the biopolymer content, as we found a larger decrease in the G' value for the 5% CSMA-15% HA-pNIPAAM bioink compared to the bioink based on 2% HAMA. Smaller molecular weight biopolymers might allow for an even higher biopolymer content while still maintaining good mechanical integrity of the bioink after thermal gelation, however, differences in polymer structure and solubility also play a role. Biopolymers have been shown to influence the gelation temperature of other thermo-gelling materials [47], however, the gelation temperature is normally increased instead of decreased as in the case of CSMA-HA-pNIPAAM. It has been found that salts disrupt the hydration structure surrounding pNIPAAM and therefore decreasing the LCST with increasing salt concentration [48]. The most effective kosmotrop according to the Hofmeister series is the sulfate

ion [49, 50]. Although not present in their ionic form, sulfate groups are abundant in CSMA and therefore might influence the gelation temperature of HA-pNIPAAM in a similar manner (Fig. 3c). The negative charge of HAMA did not seem to influence the gelation temperature to a similar extent at the concentration we used in this study as the carboxylic acid groups on the HA might not be strong enough to disturb the water structure around pNIPAAM. The overall higher charge density of chondroitin sulfate might also contribute to stronger decrease in the LCST.

Although many bioprinting approaches use bioinks which contain cells, the effect of the cells on the rheological properties is not often studied and can impact the viscosity and moduli to an unexpected extent [18]. As such the addition of cells could influence final strand diameters and printing fidelity. In the case of our bioinks, the cells changed the moduli after temperature gelation as shown in Fig. 3d. In general, we expected that the inclusion of cells would lead to a lower overall network density and a reduction of the storage modulus, as was the case for both bioinks. In case of the HAMA-HA-pNIPAAM, the storage modulus decreased from 285 to 117 Pa with the addition of cells. The way how cells influence the moduli after UV crosslinking is currently unclear. The modulus of CSMA-HA-pNIPAAM after UV crosslinking was not affected by cells, leading to the conclusion that the overall network density is only slightly lowered by the cells. For the HAMA-HA-pNIPAAM, however, the post-UV modulus is higher with cells than without. Specific interactions between the cells and the biopolymer could be a possible explanation.

Because resolution is important in bioprinting to achieve accurate spatial distribution of materials and cells, the swelling ratio of hydrogels needs to be considered. If hydrogels swell too much, the intended spatial organization might be lost. For the two bioinks presented here, the CSMA-HA-pNIPAAM bioink swelled more than the HAMA-HA-pNIPAAM (Fig. 4). The reason for this is likely due to the presence of the sulfate groups in the CSMA which leads to higher ingress of water into the hydrogel. At 4°C, the swelling of both bioinks increased over the course of the first 24 h as the HA-pNIPAAM diffuses out of the hydrogel, creating an open porous structure. The stability of swelling ratio after 24 h indicates that HA-pNIPAAM has diffused completely out of the hydrogel network by

this time. As the HAMA-based bioink swelled less than the CSMA one, it was chosen for the printing experiments.

When viability of cells cultured on top of the hydrogels was studied, we observed cluster formation in all samples indicating poor cell adhesion to the substrate. This was rather surprising as the chondrocytes should be able to interact with HA via CD44 receptors. The MTS assay (Fig. 6d) in conjunction with the live/dead staining lead us, however, to conclude that the drop in viability for the surface cells is caused by the detachment of cells rather than actual toxicity of the materials. We suspect that, due to the swelling exhibited by CSMA-HA-pNIPAAM and to a lesser extent HAMA-HA-pNIPAAM, the cells became mechanically detached from the substrate and were then removed from the surface during media exchange or the staining process (Fig. 6b and c). Contrary to top culture viability, cells did not survive over 4 days when cultured within the HAMA-HA-pNIPAAM bioink. As we suspected that the low viability was caused by limited diffusion in the highly concentrated hydrogels (Fig. 7a), HA-pNIPAAM was intentionally removed from the hydrogels by short culture at 4°C. This washing, which was visualized by a rapid increase in transparency of the scaffolds, increased the cell viability from 34% to 91% at day seven with respect to the positive control (Fig. 7a). The only regions showing cell death in the printed constructs was at the edge of the strands, which might have dried out during the printing. A humidified atmosphere during the printing process could solve this problem. The fact that the printed constructs were still mechanically stable after the elution of the HA-pNIPAAM confirms that the formation of two interpenetrated networks took place during the tandem gelation and that the second, chemically crosslinked network is alone stable enough to maintain the structure of the 3D printed constructs.

Most hydrogels used in cartilage engineering have a modulus approximately an order of magnitude lower than native cartilage [51]. For cartilage engineering, where the goal is often to trigger the repair process, one has to balance the mechanical stiffness requirements against the need for a permeable open network which promotes exchange of nutrients and oxygen. HAMA is an interesting material from this perspective because its long term in vitro and in vivo longevity can be widely

tuned by adjusting the crosslinking density of the scaffolds [52, 53]. The ability to print pure HAMA gels as demonstrated in this manuscript further extends the versatility of this class of materials.

5. Conclusion

A novel concept for 3D bioprinting with good resolution and high cell viability is introduced, based on the extrusion of a blend of a thermoresponsive polymer and a photocrosslinkable biopolymer. The two polymer system was composed of HA-pNIPAAM, which has a LCST between 25.7°C - 29.7°C, and hyaluronan methacrylate (HAMA) or chondroitin sulfate methacrylate (CSMA), which gelled in the presence of a photoinitiator and UV light. The blend showed rapid gelation upon contact with a 37°C heated substrate giving the printed construct its immediate structural fidelity, while the secondary chemical crosslinking of the co-extruded HAMA or CSMA component gave it its long-term mechanical stiffness (Fig. 2). We showed that the charge and concentration of the additional biopolymers and the presence of cells all influenced the gelation temperature and final storage modulus of the construct, but still allowed for a highly printable system. We demonstrated that the materials used for the bioinks have no direct toxicity to cells cultured on their surface. On the contrary, embedding the cells in the bioink led to high cell death most probably due to diffusion limitations of the highly crosslinked system. By removing the HA-pNIPAAM in a brief 4°C washing step (Fig. 2c), we could fabricate 3D constructs with 7 day viability which was 91% of the positive control. The great improvement in cell viability was likely due to the creation of a more open, porous network which enhanced diffusion. To conclude, HA-pNIPAAM can be used as a transient support polymer to facilitate 3D printing at physiologic temperature of a range of biopolymer solutions which would otherwise not be printable.

Acknowledgements

The work was partially funded by the European Union Seventh Framework Programme (FP7/2007-

2013) under grant agreement n°NMP4-SL-2009-229292, the Swiss National Science Foundation (grant number CR32I3_146338 / 1), AO Foundation (Grant number S-11-60Z), and Fifa. We thank Rami Mhanna for scientific advice, Albrecht Berg for providing the photoinitiator LAP, Gert-Jan Ter Boo for providing HA-pNIPAAM material support, and Anne-Kathrin Born and Florian Formica for help in revising the manuscript.

Figure Captions

Figure 1. a) The variation in G'/G'' is schematically illustrated for the different stages of bioprinting with a thermoresponsive polymer. b) The gelation mechanism in which HA-pNIPAAM forms a physical gel (only the isopropyl groups of pNIPAAM are depicted).

Figure 2. Schematic illustration of the fabrication of 3D constructs for cartilage engineering: a) Thermal crosslinking of the bioink maintains the printed shape b) Establishment of a mechanically stable secondary network with UV crosslinking c) Elution of the transient matrix d) Implantation into a cartilage lesion.

Figure 3. a) HA-pNIPAAM was crosslinked by increasing the temperature by 0.5°C/min. Closed symbols represent G' (storage modulus) and open symbols G'' (loss modulus). b) Shear recovery of 15% HA-pNIPAAM at different temperatures b). In c) and d) the temperature and UV-crosslinking behavior of the bioinks HAMA-HA-pNIPAAM and CSMA-HA-pNIPAAM are shown without (c) and with (d) the addition of cells. The temperature was increased by 0.5°C/min from 4°C to 45°C during the first 92.5min. Samples were then cooled to 37°C and maintained at that temperature until the end of the measurement. All the measurements were performed in duplicate.

Figure 4. Swelling behavior of the two bioinks in PBS over 48 h. The bioinks contain 15% HA-pNIPAAM and either 2% HAMA (a) or 5% CSMA (b). The swelling of the UV crosslinked bioinks was measured at 4°C and 37°C. Error bars indicate standard deviation (n=5).

Figure 5. a) Top view and b) angled view of the HAMA-HA-pNIPAAM printed scaffolds. The height of the printed scaffolds was 2.8 mm from 14 printed layers. The crosslinked constructs were stable enough be picked up from the substrate and handled with a spatula c). The scaffold is opaque at 37°C and becomes transparent at room temperature.

Figure 6. Chondrocyte viability after 7 days of culture on top of bioink hydrogels. a) 15% HA-pNIPAAM (HAp). Cells are present in clusters, which can also be seen on HAMA-HA-pNIPAAM (HAMA HAp) b). c) CSMA-HA-pNIPAAM (CSMA HAp) showed mostly detached cells. An MTS assay after 7 days with cells cultured on top of different hydrogels is shown in d) with 1% alginate (1% Alg) as a positive control and measurements were performed in duplicate. *$p<0.01$ and **$p<0.001$, Scale bar = 200 µm.

Figure 7. a) Chondrocyte viability after 14 days of culture within printed HAMA-HA-pNIPAAM scaffolds with unwashed (before HAp removal 7 days) and washed (after HAp removal 4-14 days) conditions. 70% ethanol and 1% alginate (1% Alg) were used as negative and positive controls and all measurements were performed in duplicate. b) and c) Low and high magnification of Live/Dead staining of the printed and washed HAMA-HA-pNIPAAM scaffolds after 4 days. Increased cell death around the pores is visible. d) The unwashed scaffolds have an opaque appearance at 37°C indicating the presence of gelled HA-pNIPAAM (left image) while washed scaffolds were transparent (right). Scale bars are 1 mm (b) and 200 µm (c). *<0.05, **<0.001

Supplementary Figure S1. Live dead image of cells encapsulated in 1% alginate after 4 days in culture.

Supplementary Figure S2. MTS viability data from chondrocytes encapsulated in alginate. UV exposure for 90 seconds did not have any influence on the viability of the cells.

References

[1] Buckwalter JA, Mankin HJ, Grodzinsky AJ. Articular cartilage and osteoarthritis. Instructional course lectures - american academy of orthopaedic surgeons 2005;54:465.
[2] Roos EM. Joint injury causes knee osteoarthritis in young adults. Curr Opin Rheumatol 2005;17:195-200.
[3] Krych AJ, Harnly HW, Rodeo SA, Williams RJ, 3rd. Activity levels are higher after osteochondral autograft transfer mosaicplasty than after microfracture for articular cartilage defects of the knee: a retrospective comparative study. J Bone Joint Surg Am 2012;94:971-978.
[4] Hangody L, Dobos J, Baló E, Pánics G, Hangody LR, Berkes I. Clinical Experiences With Autologous Osteochondral Mosaicplasty in an Athletic Population: A 17-Year Prospective Multicenter Study. The American Journal of Sports Medicine 2010;38:1125-1133.
[5] Chen FH, Rousche KT, Tuan RS. Technology Insight: adult stem cells in cartilage regeneration and tissue engineering. Nat Clin Pract Rheum 2006;2:373-382.
[6] Klein TJ, Rizzi SC, Schrobback K, Reichert JC, Jeon JE, Crawford RW, et al. Long-term effects of hydrogel properties on human chondrocyte behavior. Soft Matter 2010;6:5175-5183.
[7] Xu T, Jin J, Gregory C, Hickman JJ, Boland T. Inkjet printing of viable mammalian cells. Biomaterials 2005;26:93-99.
[8] Mhanna R, Kashyap A, Palazzolo G, Vallmajo-Martin Q, Becher J, Moller S, et al. Chondrocyte Culture in Three Dimensional Alginate Sulfate Hydrogels Promotes Proliferation While Maintaining Expression of Chondrogenic Markers. Tissue engineering Part A 2014; doi: 10.1089/ten.TEA.2013.0544.
[9] Yan L-P, Oliveira JM, Oliveira AL, Caridade SG, Mano JF, Reis RL. Macro/microporous silk fibroin scaffolds with potential for articular cartilage and meniscus tissue engineering applications. Acta Biomater 2012;8:289-301.
[10] Khalil S, Sun W. Bioprinting Endothelial Cells With Alginate for 3D Tissue Constructs. Journal of Biomechanical Engineering 2009;131:1110021-1110028.
[11] Madry H, Rey-Rico A, Venkatesan JK, Johnstone B, Cucchiarini M. Transforming Growth Factor Beta-Releasing Scaffolds for Cartilage Tissue Engineering. Tissue Eng Part B Rev 2013;20:106-125.
[12] Spiller KL, Liu Y, Holloway JL, Maher SA, Cao Y, Liu W, et al. A novel method for the direct fabrication of growth factor-loaded microspheres within porous nondegradable hydrogels: Controlled release for cartilage tissue engineering. J Controlled Release 2012;157:39-45.
[13] Mhanna R, Ozturk E, Vallmajo-Martin Q, Millan C, Muller M, Zenobi-Wong M. GFOGER-Modified MMP-Sensitive Polyethylene Glycol Hydrogels Induce Chondrogenic Differentiation of Human Mesenchymal Stem Cells. Tissue engineering Part A 2014;20:1165-1174.
[14] Jakab K, Neagu A, Mironov V, Forgacs G. Organ printing: fiction or science. Biorheology 2004;41:371-375.
[15] Pataky K, Braschler T, Negro A, Renaud P, Lutolf MP, Brugger J. Microdrop Printing of Hydrogel Bioinks into 3D Tissue-Like Geometries. Advanced Materials 2012;24:391-396.
[16] Hoch E, Hirth T, Tovar GEM, Borchers K. Chemical tailoring of gelatin to adjust its chemical and physical properties for functional bioprinting. Journal of Materials Chemistry B 2013;1:5675-5685.

[17] Pescosolido L, Vermonden T, Malda J, Censi R, Dhert WJA, Alhaique F, et al. In situ forming IPN hydrogels of calcium alginate and dextran-HEMA for biomedical applications. Acta Biomater 2011;7:1627-1633.
[18] Billiet T, Gevaert E, De Schryver T, Cornelissen M, Dubruel P. The 3D printing of gelatin methacrylamide cell-laden tissue-engineered constructs with high cell viability. Biomaterials 2014;35:49-62.
[19] Müller M, Becher J, Schnabelrauch M, Zenobi-Wong M. Printing Thermoresponsive Reverse Molds for the Creation of Patterned Two-component Hydrogels for 3D Cell Culture. JoVE (Journal of Visualized Experiments) 2013:e50632-e50632.
[20] Chung JHY, Naficy S, Yue ZL, Kapsa R, Quigley A, Moulton SE, et al. Bio-ink properties and printability for extrusion printing living cells. Biomater Sci-Uk 2013;1:763-773.
[21] Li SJ, Yan YN, Xiong Z, Weng CY, Zhang RJ, Wang XH. Gradient Hydrogel Construct Based on an Improved Cell Assembling System. J Bioact Compatible Polym 2009;24:84-99.
[22] Schuurman W, Levett PA, Pot MW, van Weeren PR, Dhert WJA, Hutmacher DW, et al. Gelatin-Methacrylamide Hydrogels as Potential Biomaterials for Fabrication of Tissue-Engineered Cartilage Constructs. Macromol Biosci 2013;13:551-561.
[23] Fedorovich NE, Swennen I, Girones J, Moroni L, van Blitterswijk CA, Schacht E, et al. Evaluation of Photocrosslinked Lutrol Hydrogel for Tissue Printing Applications. Biomacromolecules 2009;10:1689-1696.
[24] Maher PS, Keatch RP, Donnelly K, Mackay RE, Paxton JZ. Construction of 3D biological matrices using rapid prototyping technology. Rapid Prototyping J 2009;15:204-210.
[25] Malda J, Visser J, Melchels FP, Jungst T, Hennink WE, Dhert WJA, et al. 25th Anniversary Article: Engineering Hydrogels for Biofabrication. Advanced Materials 2013;25:5011-5028.
[26] Chung C, Burdick JA. Influence of three-dimensional hyaluronic acid microenvironments on mesenchymal stem cell chondrogenesis. Tissue engineering Part A 2009;15:243-254.
[27] Wang DA, Varghese S, Sharma B, Strehin I, Fermanian S, Gorham J, et al. Multifunctional chondroitin sulphate for cartilage tissue-biomaterial integration. Nature Materials 2007;6:385-392.
[28] Kim IL, Mauck RL, Burdick JA. Hydrogel design for cartilage tissue engineering: A case study with hyaluronic acid. Biomaterials 2011;32:8771-8782.
[29] Levett PA, Melchels FPW, Schrobback K, Hutmacher DW, Malda J, Klein TJ. A biomimetic extracellular matrix for cartilage tissue engineering centered on photocurable gelatin, hyaluronic acid and chondroitin sulfate. Acta Biomater 2014;10:214-223.
[30] Kataoka Y, Ariyoshi W, Okinaga T, Kaneuji T, Mitsugi S, Takahashi T, et al. Mechanisms involved in suppression of ADAMTS4 expression in synoviocytes by high molecular weight hyaluronic acid. Biochem Biophys Res Commun 2013;432:580-585.
[31] Jomphe C, Gabriac M, Hale TM, Heroux L, Trudeau LE, Deblois D, et al. Chondroitin sulfate inhibits the nuclear translocation of nuclear Factor-kappa B in interleukin-1 beta-stimulated chondrocytes. Basic Clin Pharmacol Toxicol 2008;102:59-65.
[32] Iovu M, Dumais G, du Souich P. Anti-inflammatory activity of chondroitin sulfate. Osteoarthritis Cartilage 2008;16 Suppl 3:S14-18.
[33] Hanson SE, King SN, Kim J, Chen X, Thibeault SL, Hematti P. The effect of mesenchymal stromal cell-hyaluronic acid hydrogel constructs on immunophenotype of macrophages. Tissue engineering Part A 2011;17:2463-2471.
[34] Peroglio M, Grad S, Mortisen D, Sprecher CM, Illien-Jünger S, Alini M, et al. Injectable thermoreversible hyaluronan-based hydrogels for nucleus pulposus cell encapsulation. European Spine Journal 2012;21:839-849.

[35] Peroglio M, Eglin D, Benneker LM, Alini M, Grad S. Thermoreversible hyaluronan-based hydrogel supports in vitro and ex vivo disc-like differentiation of human mesenchymal stem cells. The Spine Journal 2013;13:1627-1639.
[36] Mortisen D, Peroglio M, Alini M, Eglin D. Tailoring thermoreversible hyaluronan hydrogels by “click” chemistry and RAFT polymerization for cell and drug therapy. Biomacromolecules 2010;11:1261-1272.
[37] Peroglio M, Eglin D, Benneker LM, Alini M, Grad S. Thermoreversible hyaluronan-based hydrogel supports in vitro and ex vivo disc-like differentiation of human mesenchymal stem cells. The spine journal : official journal of the North American Spine Society 2013;13:1627-1639.
[38] D'Este M, Alini M, Eglin D. Single step synthesis and characterization of thermoresponsive hyaluronan hydrogels. Carbohydrate Polymers 2012;90:1378-1385.
[39] Chiantore O, Guaita M, Trossarelli L. Solution Properties of Poly(N-Isopropylacrylamide). Makromolekulare Chemie-Macromolecular Chemistry and Physics 1979;180:969-973.
[40] Fairbanks BD, Schwartz MP, Bowman CN, Anseth KS. Photoinitiated polymerization of PEG-diacrylate with lithium phenyl-2,4,6-trimethylbenzoylphosphinate: polymerization rate and cytocompatibility. Biomaterials 2009;30:6702-6707.
[41] Muramatsu K, Ide M, Miyawaki F. Biological Evaluation of Tissue-Engineered Cartilage Using Thermoresponsive Poly (N-isopropylacrylamide)-Grafted Hyaluronan. Journal of Biomaterials & Nanobiotechnology 2012;3.
[42] Wong M, Siegrist M, Wang XH, Hunziker E. Development of mechanically stable alginate/chondrocyte constructs: effects of guluronic acid content and matrix synthesis. J Orth Res 2001;19:493-499.
[43] Hauselmann HJ, Fernandes RJ, Mok SS, Schmid TM, Block JA, Aydelotte MB, et al. Phenotypic Stability of Bovine Articular Chondrocytes after Long-Term Culture in Alginate Beads. J Cell Sci 1994;107:17-27.
[44] Wust S, Godla ME, Muller R, Hofmann S. Tunable hydrogel composite with two-step processing in combination with innovative hardware upgrade for cell-based three-dimensional bioprinting. Acta Biomater 2014;10:630-640.
[45] Cellesi F, Tirelli N, Hubbell JA. Materials for cell encapsulation via a new tandem approach combining reverse thermal gelation and covalent crosslinking. Macromolecular Chemistry and Physics 2002;203:1466-1472.
[46] Larson RG. The structure and rheology of complex fluids. New York: Oxford University Press; 1999.
[47] Yoo HS. Photo-cross-linkable and thermo-responsive hydrogels containing chitosan and Pluronic for sustained release of human growth hormone (hGH). Journal of Biomaterials Science-Polymer Edition 2007;18:1429-1441.
[48] Van Durme K, Rahier H, Van Mele B. Influence of additives on the thermoresponsive behavior of polymers in aqueous solution. Macromolecules 2005;38:10155-10163.
[49] Hofmeister F. On the understanding of the effects of salts. Arch Exp Pathol Pharmakol(Leipzig) 1888;24:247-260.
[50] Zhang Y, Furyk S, Bergbreiter DE, Cremer PS. Specific ion effects on the water solubility of macromolecules: PNIPAM and the Hofmeister series. J Am Chem Soc 2005;127:14505-14510.
[51] Gigante A, Bevilacqua C, Zara C, Travasi M, Chillemi C. Autologous chondrocyte implantation: cells phenotype and proliferation analysis. Knee surgery, sports traumatology, arthroscopy : official journal of the ESSKA 2001;9:254-258.

[52] Tous E, Ifkovits JL, Koomalsingh KJ, Shuto T, Soeda T, Kondo N, et al. Influence of injectable hyaluronic acid hydrogel degradation behavior on infarction-induced ventricular remodeling. Biomacromolecules 2011;12:4127-4135.
[53] Burdick JA, Chung C, Jia X, Randolph MA, Langer R. Controlled degradation and mechanical behavior of photopolymerized hyaluronic acid networks. Biomacromolecules 2005;6:386-391.

Figure 1

Click here to download high resolution image

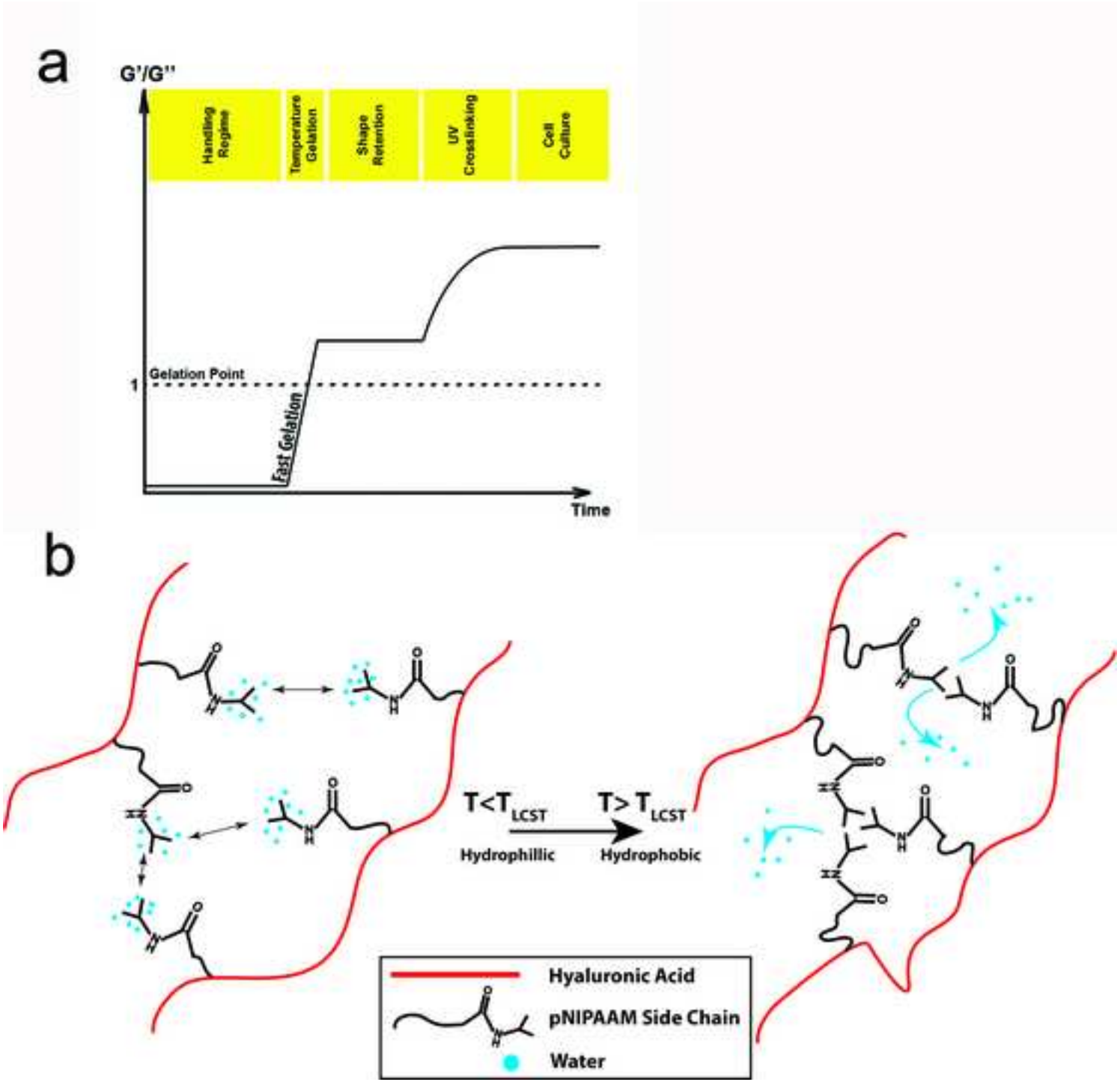

Figure 2

Click here to download high resolution image

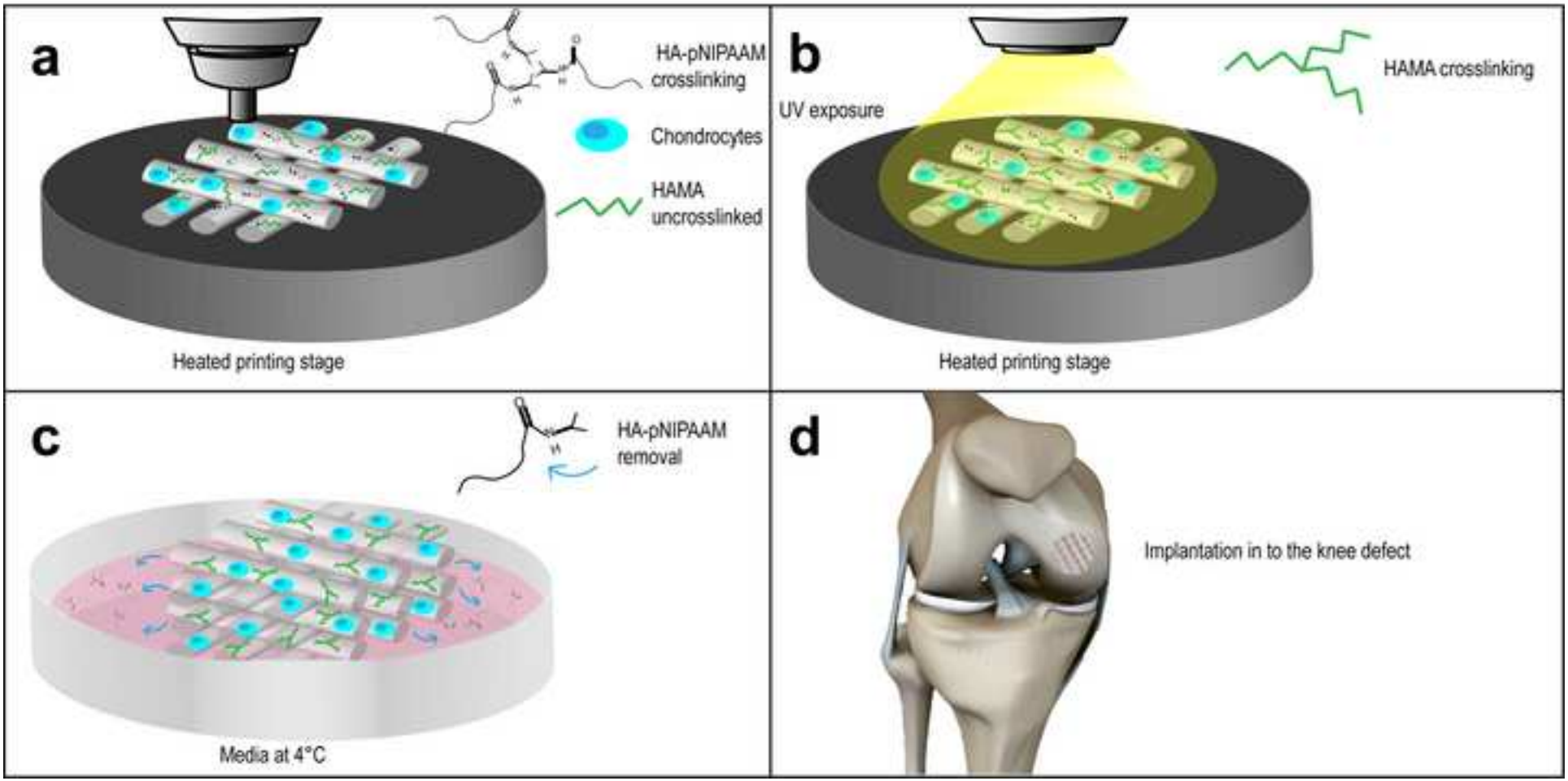

Figure 3

Click here to download high resolution image

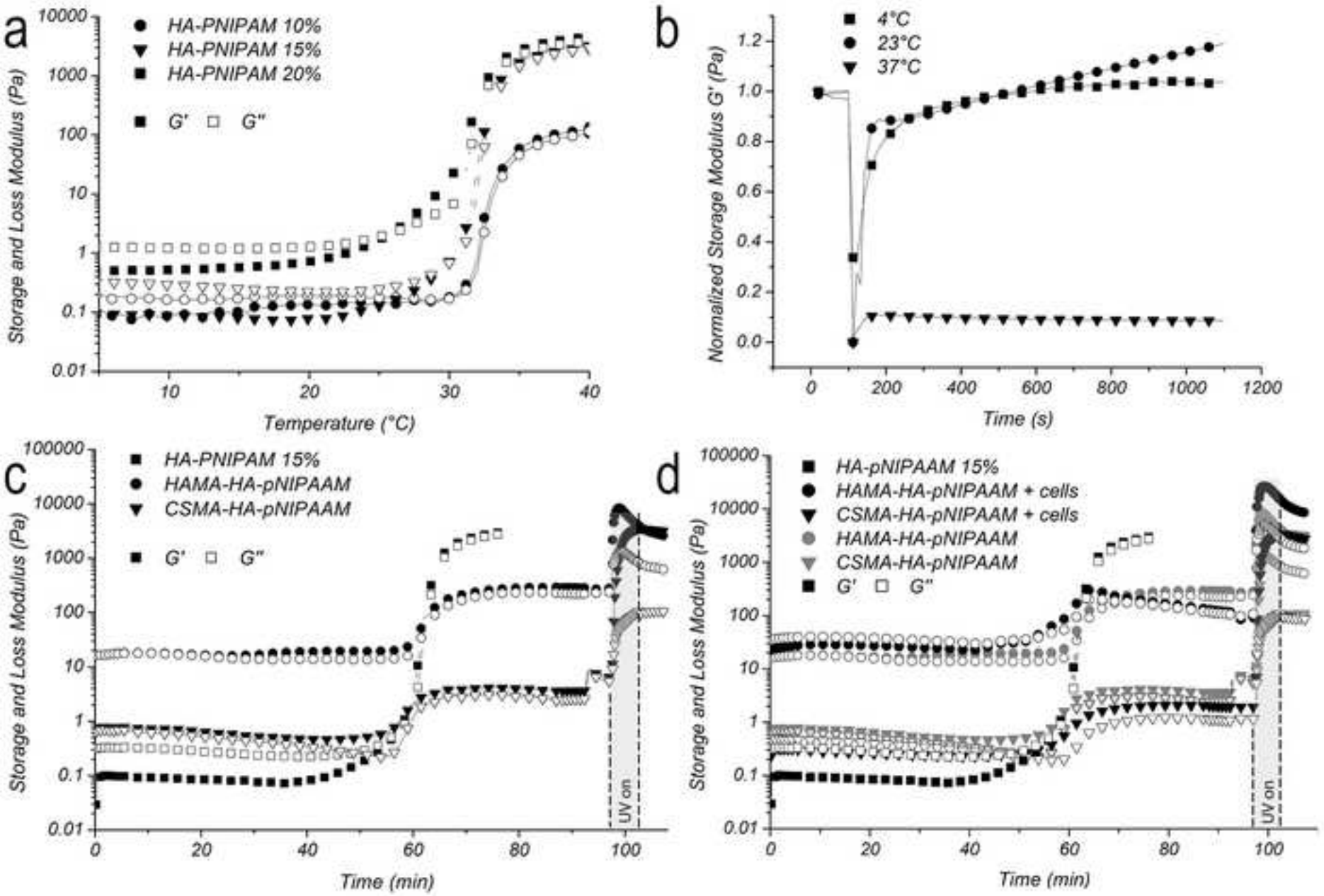

Figure 4

Click here to download high resolution image

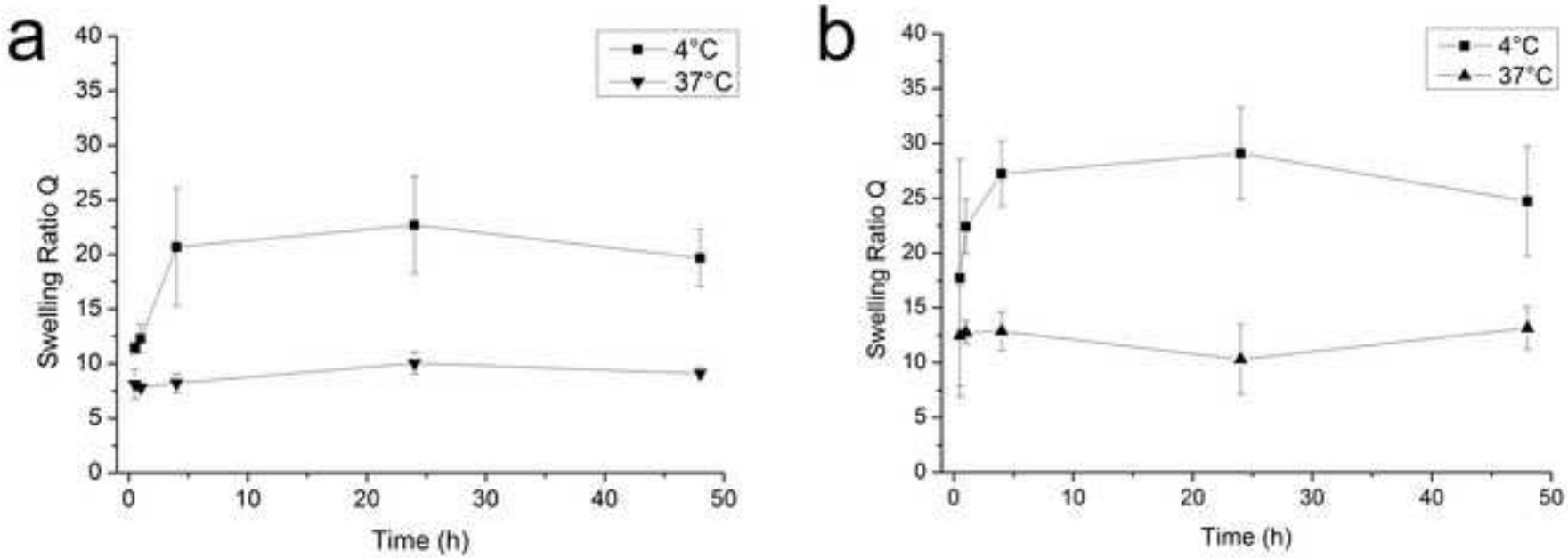

Figure 5

Click here to download high resolution image

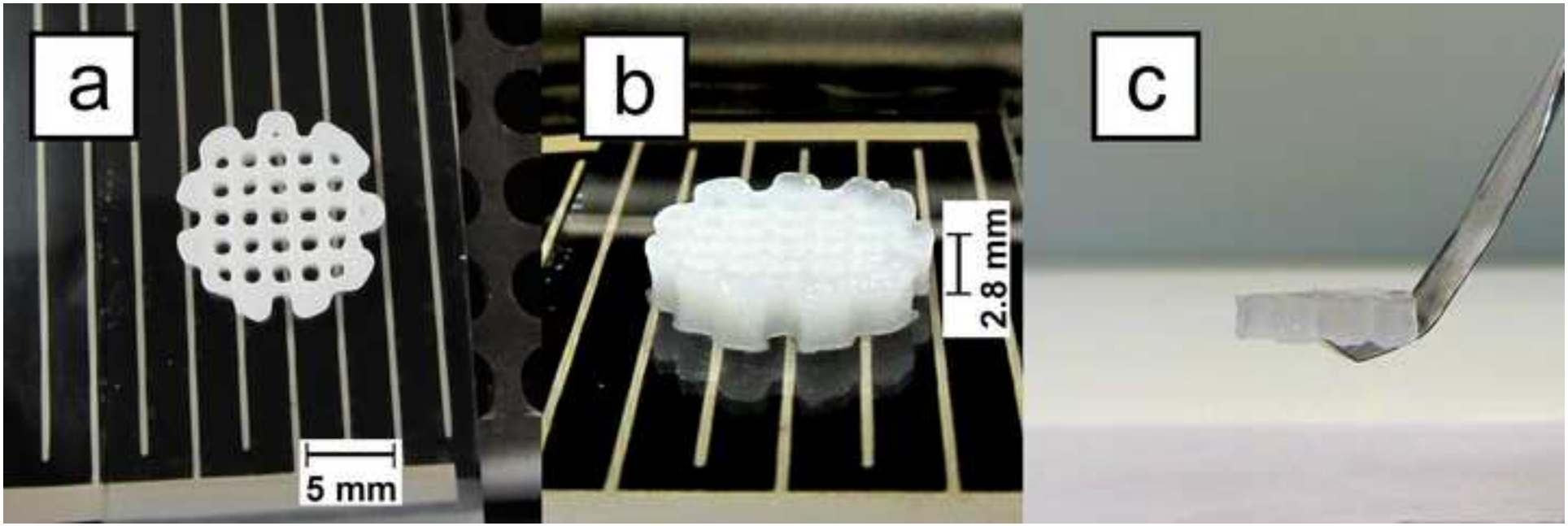

Figure 6

Click here to download high resolution image

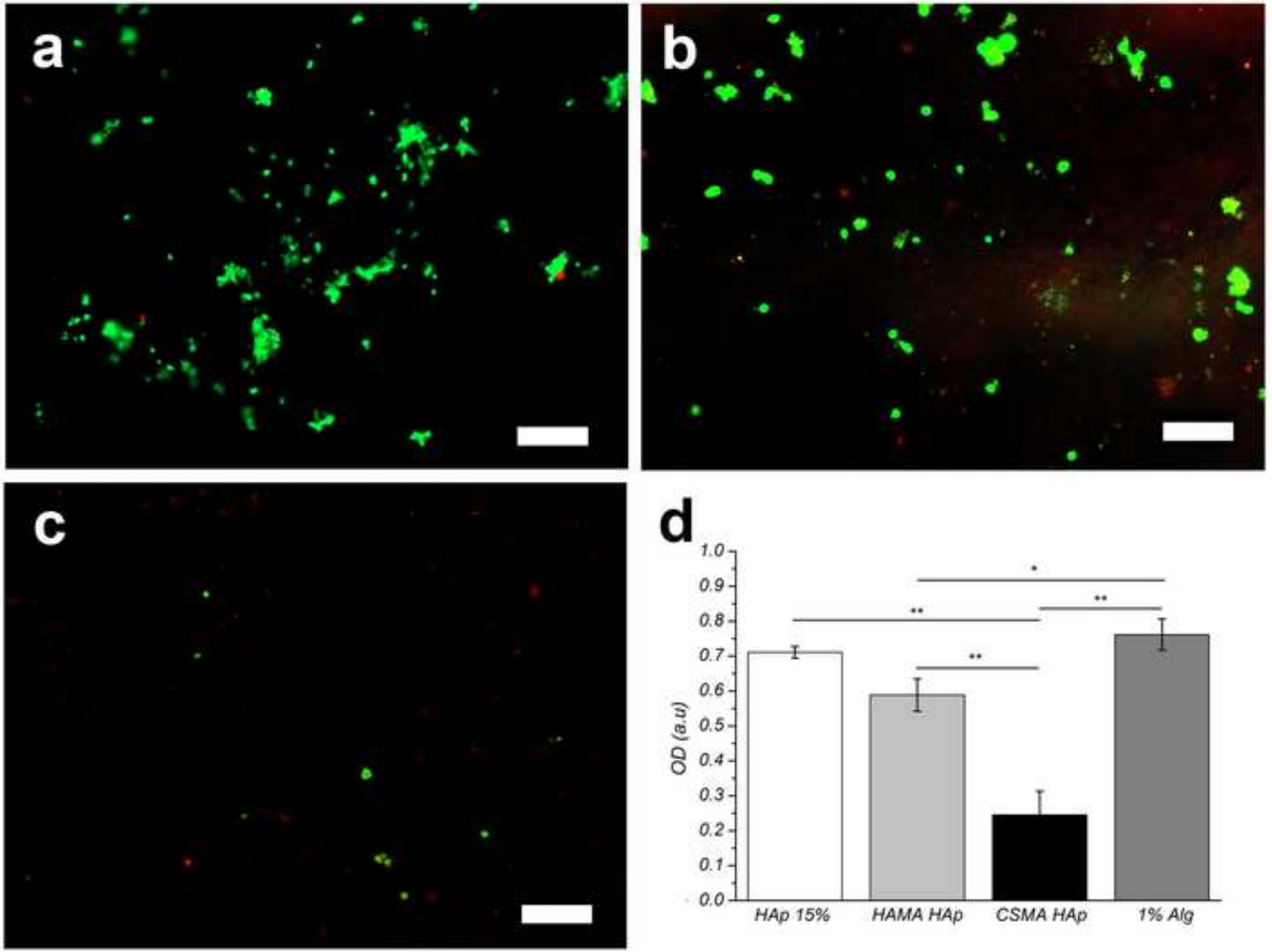

Figure 7

Click here to download high resolution image

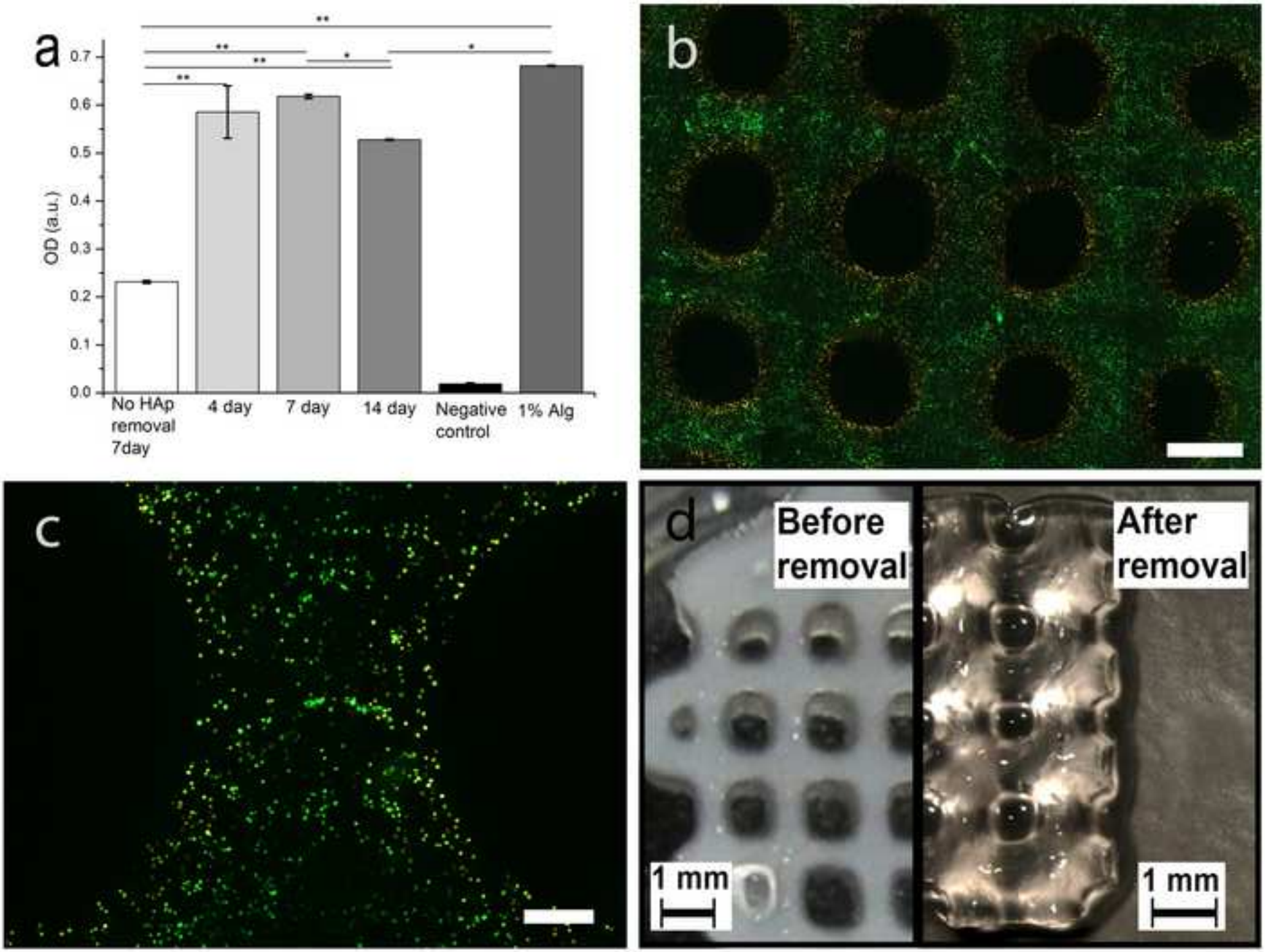

Figure S1

Click here to download high resolution image

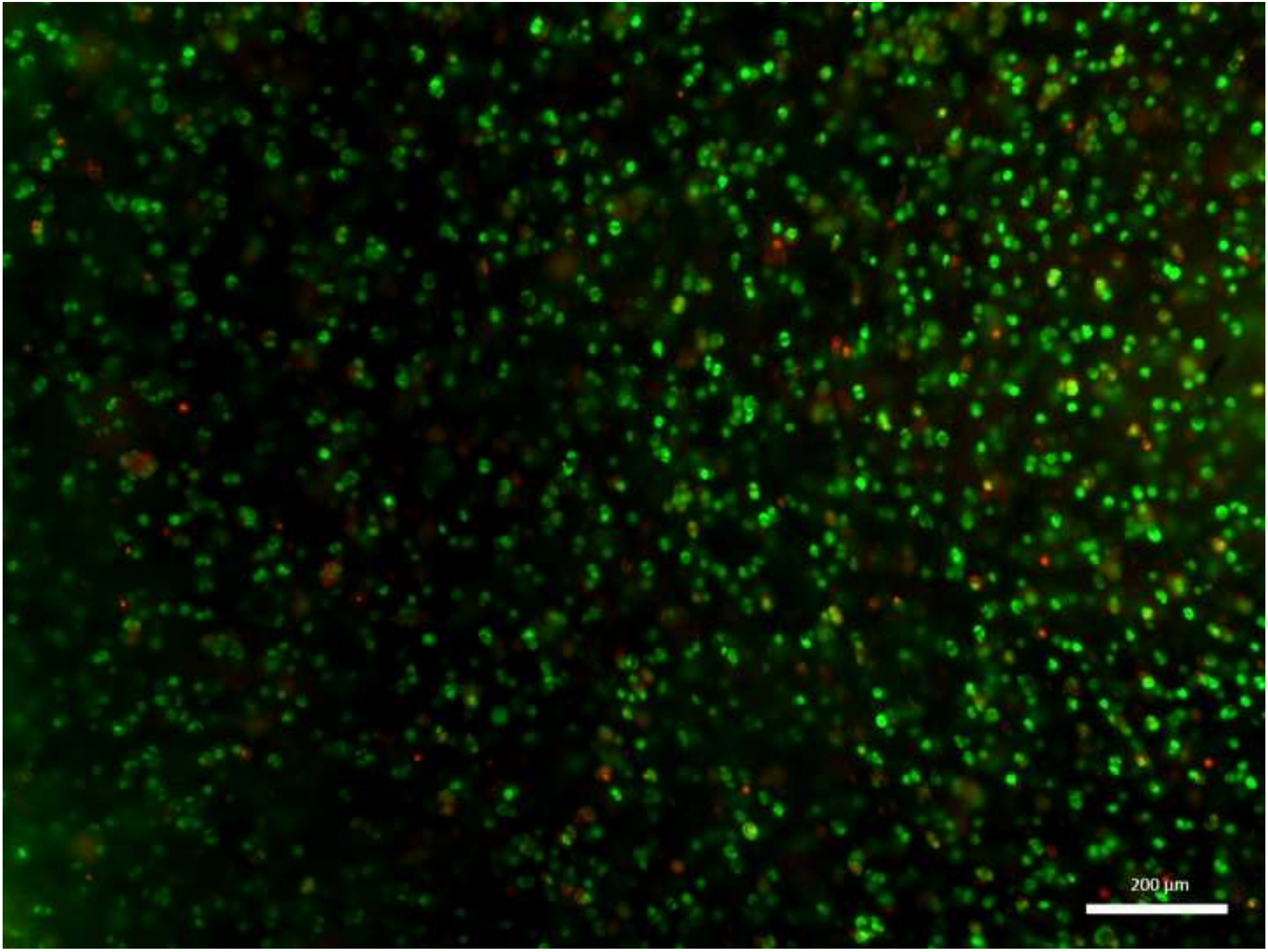

Figure S2

Click here to download high resolution image

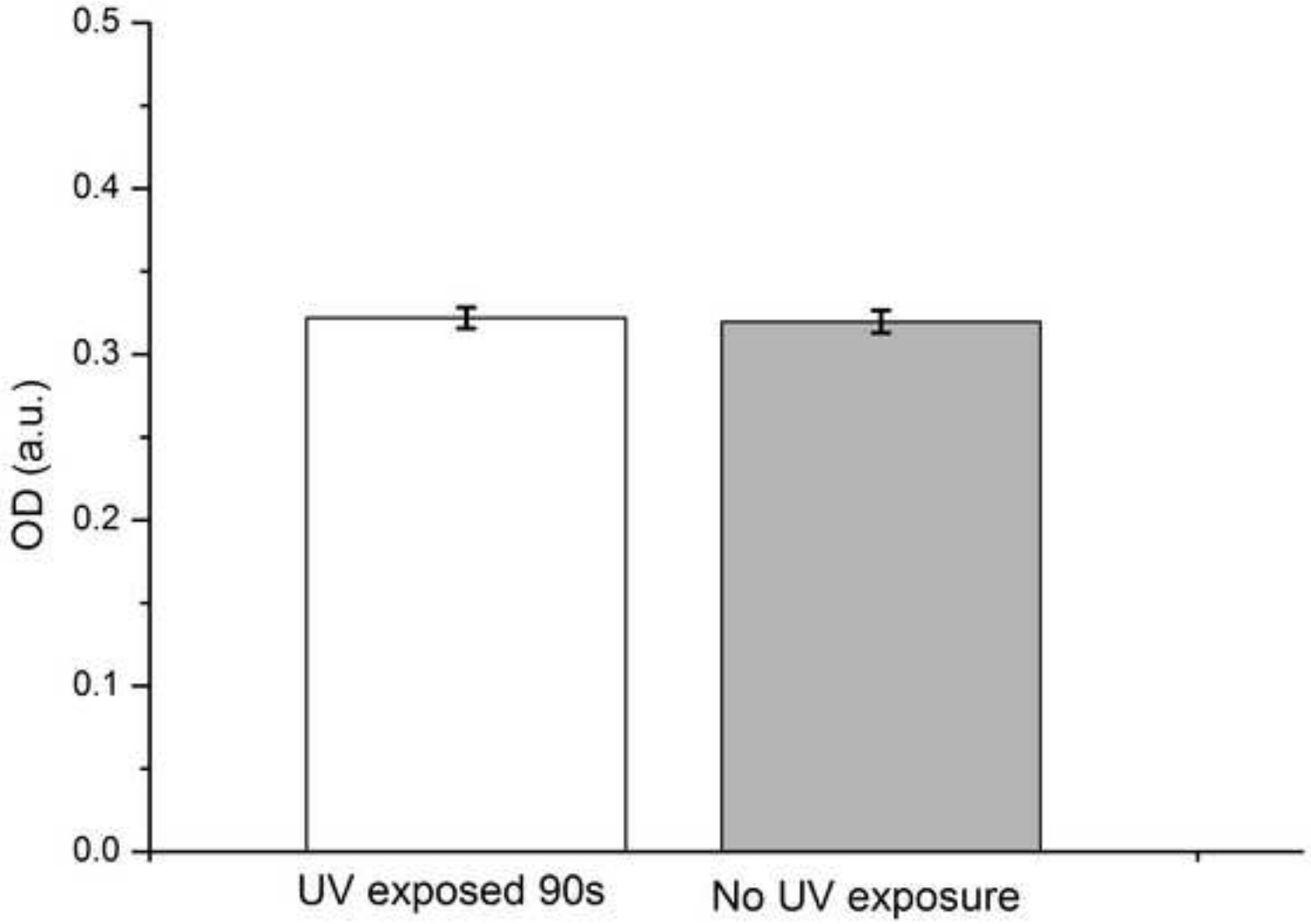

***Graphical Abstract**